Diffraction of Sound Waves from Cavity with Inner Lining and Wall Thickness

B. Tiryakioglu*

Department of Mathematics, Marmara University, 34722 Istanbul, Turkey

Received: 11.02.2022 & Accepted: 04.04.2022

Doi: 10.12693/APhysPolA.141.602 *e-mail: burhan.tiryakioglu@marmara.edu.tr

By applying the Wiener–Hopf and mode matching technique, the diffraction of sound waves by a circular cylindrical cavity with an inner lining is analyzed. In this study, it is assumed that the pipe walls are of a certain thickness, which makes the problem more interesting. Problems in which it is usually assumed that the walls are infinitely thin are not realistic for modeling, since in practice every wall has a certain thickness. While solving our case, an infinite system of algebraic equations is obtained, and the system is solved numerically by truncating to the certain numbers. Finally, graphs of some parameters, such as cavity thickness and depth, are produced for the diffracted field phenomenon, and the consistency of the results is compared with a study available in the literature.

topics: cavity, wall thickness, Wiener–Hopf

1. Introduction

In recent years, researchers working in the fields of mathematics, physics, and engineering have been very interested in the problem of reducing noise resulting from various reasons. The pipe outlet is an important area of noise reduction research. Scientists have been investigating this problem for years [1–5]. Sound absorbing linings are one of the most effective methods of reducing the generated noise.

The cavity problem is a field of study that attracts attention in acoustics and electromagnetism [6–9]. It is applicable in areas such as microphones, radar cross-sections, and turbofan engine intakes. Some cavity diffraction problems have been investigated by researchers using various methods.

Different methods can be used to solve scattering problems. In geometries with many discontinuity points, which may be an expansion-contraction chamber or non-uniform lining, the scattering matrix technique may be particularly preferred. It is also a very effective method for an acoustic system consisting of multi-mode multi-ports [10–12].

Levine and Schwinger [13] analyzed the radiation of sound waves from a semi-infinite duct with rigid walls using the Wiener–Hopf technique [14]. Ando [15] analyzed the radiation of sound waves by a semi-infinite circular duct of a certain wall thickness, using Laplace transforms and the Wiener–Hopf technique. Rawlins [16] proved that acoustic absorbing linings are an effective method of suppressing unwanted noise. He analyzed the sound radiation from the duct, whose inner surface is lined with an absorbing lining and the outer surface is rigid. The diffraction of acoustic waves from a semi-infinite duct with a certain wall thickness was studied in detail by Polat and Buyukaksoy [17]. In their study, a ring source was used to illuminate the duct, and they considered that both the inside, the outside, and the end of the duct were covered with acoustically absorbing lining. The diffraction of sound waves from a cavity located in a semi-infinite cylindrical pipe was analyzed rigorously by Demir et al. [18]. In their study, in which both the inside and the bottom of the cavity were lined, it was assumed that the walls were infinitely thin. Especially in acoustic problems, Wiener–Hopf and mode matching techniques are widely used [19–22].

Most of the studies are limited to infinitely thin pipe walls. In practice, it is unrealistic to model them as infinitely thin, because each cylindrical pipe/duct has a wall thickness. For this reason, the wall thickness will affect the diffraction phenomenon [15, 17].

Considering the above-mentioned studies, the present study aims to analyze the effects of cavity wall thickness on the diffraction phenomenon. The geometry, which consists of a semi-infinite circular cylindrical cavity with a wall thickness and an incident field, of the problem currently under consideration is displayed in Fig. 1. The wall thickness makes the problem interesting when considering an infinitely thin wall. By applying the Wiener–Hopf technique, which is one of the most

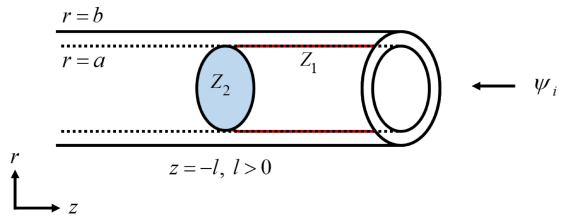

Fig. 1. Geometry of the problem.

suitable methods for propagation problems, and using the Fourier transform, the relevant boundary value problem is solved analytically. As a result of solving the Wiener–Hopf equation, a system of equations with an infinite number of unknown coefficients is obtained. This system is truncated to a certain number, and the solution is found approximately. Incorporating the wall thickness into the problem causes changes in the points of continuity. Therefore, rigorous analysis is required to obtain the solution. One of our most important goals in this study is to understand the effect of cavity wall thickness on the diffraction phenomenon.

The accuracy of the results of the this study is obtained by comparing them with another study in the literature [18]. In the graphics obtained by taking the wall thickness to zero, a very good agreement is seen.

2. Problem statement

Consider the diffraction of sound waves in a cavity located at $r = a$ and $z \in (-l, 0)$, formed by a semi-infinite cylindrical waveguide that occupies the region $\{r = b, z \in (-\infty, 0)\}$. The outer surface of the cylinder is assumed to be rigid, while the inner surface and the base of the cavity are assumed to be lined with acoustically absorbing materials. The liner impedance is characterized by Z_1 and Z_2, respectively. Since the incident field and the geometry of the problem are symmetrical, the total field is independent of ϕ in the circular cylindrical coordinate system (r, ϕ, z). Therefore, the acoustic pressure $p = \mathrm{i}\omega\rho_0\psi$ and the velocity $\boldsymbol{v} = \nabla\psi$ are defined with the help of a scalar $\psi(r, z)$ function. In this study, in which the time dependence is considered as $\mathrm{e}^{-\mathrm{i}\omega t}$, ρ_0 indicates the density of the undisturbed medium, and ω indicates the angular frequency.

The incident sound wave, which is assumed to propagate in the negative z-direction, is taken as

$$\psi_i(z) = \mathrm{e}^{-\mathrm{i}kz}, \tag{1}$$

where $k = \omega/c$ indicates the wave number and c is the speed of sound. The expression of the total field will be formed as follows

$$\psi^T(r, z) = \begin{cases} \psi_1(r, z) + \psi_i(z); & r > b,\ z \in \mathbb{R}, \\ \psi_2(r, z) + \psi_i(z); & r < b,\ z > 0, \\ \psi_3(r, z); & r < a, -l < z < 0, \end{cases} \tag{2}$$

where each ψ_j $(j = 1, 2, 3)$

$$\left[\frac{1}{r}\frac{\partial}{\partial r}\left(r\frac{\partial}{\partial r}\right) + \frac{\partial^2}{\partial z^2} + k^2\right]\psi_j(r, z) = 0. \tag{3}$$

Using the expression $\psi_1(r, z)$, the boundary condition over the rigid surface is obtained as

$$\frac{\partial}{\partial r}\psi_1(b, z) = 0, \quad z < 0. \tag{4}$$

The interior surface and the base of the cavity are assumed to be lined with an absorbing lining Z_1 and Z_2, respectively. It is given by

$$\left(\frac{\mathrm{i}k}{Z_1} - \frac{\partial}{\partial r}\right)\psi_3(a, z) = 0, \quad -l < z < 0, \tag{5}$$

$$\left(\frac{\mathrm{i}k}{Z_2} + \frac{\partial}{\partial z}\right)\psi_3(r, -l) = 0, \quad 0 < r < a. \tag{6}$$

The thickness of the cavity edge is assumed to be rigid, thus

$$\frac{\partial}{\partial z}\psi_2(r, 0) = 0, \quad a < r < b. \tag{7}$$

Let us now consider the continuity conditions for the total area. At $r = b$, $z > l$, one gets

$$\frac{\partial}{\partial r}\psi_1(b, z) - \frac{\partial}{\partial r}\psi_2(b, z) = 0, \quad z > 0, \tag{8}$$

$$\psi_1(b, z) - \psi_2(b, z) = 0, \quad z > 0. \tag{9}$$

From the continuity conditions at the point $z = 0$, one gets for $r < a$ the following equations

$$\frac{\partial}{\partial z}\psi_3(r, 0) = \frac{\partial}{\partial z}\psi_2(r, 0) + \frac{\partial}{\partial z}\psi_i(0), \tag{10}$$

$$\psi_3(r, 0) = \psi_2(r, 0) + \psi_i(0). \tag{11}$$

3. Derivation and solution of the Wiener–Hopf equation

The unknown field $\psi_1(r, z)$, where $r > b$ for $z \in (-\infty, \infty)$, satisfies the Helmholtz equation (3). By using Fourier transform, we get

$$\left[\frac{1}{r}\frac{\partial}{\partial r}\left(r\frac{\partial}{\partial r}\right) + K^2(\alpha)\right]F(r, \alpha) = 0, \tag{12}$$

where $K(\alpha) = \sqrt{k^2 - \alpha^2}$ is defined in the complex α-plane. Here, $F(r, \alpha)$ is obtained by taking the Fourier transform of $\psi_1(r, z)$ and is defined as follows [23]

$$F(r, \alpha) = \int_{-\infty}^{\infty} \mathrm{d}z\, \psi_1(r, z)\ \mathrm{e}^{\mathrm{i}\alpha z} =$$

$$F^-(r, \alpha) + F^+(r, \alpha). \tag{13}$$

Due to the analytical properties of Fourier integrals, $F^+(r, \alpha)$ is the analytic function of α in the upper half-plane $(\mathrm{Im}(\alpha) > \mathrm{Im}(-k))$, and $F^-(r, \alpha)$ is an analytic function in the lower half-plane $(\mathrm{Im}(\alpha) < \mathrm{Im}(k))$. The solution of (12) is

$$F^-(r, \alpha) + F^+(r, \alpha) = -\frac{\dot{F}^+(a, \alpha)\ H_0^{(1)}(Kr)}{K\, H_1^{(1)}(Kb)}, \tag{14}$$

where $H_m^{(1)}$ is the Hankel function of the first type. Here, the dot notation over a function denotes the derivative with respect to r. In the region $\{r < b, z > 0\}$, the following equation

$$\left[\frac{1}{r}\frac{\partial}{\partial r}\left(r\frac{\partial}{\partial r}\right)+K^2(\alpha)\right]G^+(r,\alpha)=f(r)-\mathrm{i}\alpha g(r) \tag{15}$$

is obtained by taking the half-range Fourier transform of the Helmholtz equation satisfied by $\psi_2(r,z)$. In (15), $G^+(r,\alpha)$ is an analytic function in the upper α-plane, and its definition is

$$G^+(r,\alpha)=\int_0^\infty \mathrm{d}z\,\psi_2(r,z)\,\mathrm{e}^{\mathrm{i}\alpha z}, \tag{16}$$

while $f(r)$ and $g(r)$ are

$$\begin{aligned} f(r)&=\tfrac{\partial}{\partial z}\psi_2(r,0),\\ g(r)&=\psi_2(r,0). \end{aligned} \tag{17}$$

By using the properties of Green's function, the solution of (15) can be written as [23]

$$G^+(r,\alpha)=\frac{1}{K\,J_1(Kb)}\left[-B(\alpha)\,J_0(Kr)+\int_0^a \mathrm{d}r'\,r'\Big(f(r')-\mathrm{i}\alpha g(r')\Big)\,Q(r',r,\alpha)\right], \tag{18}$$

where $B(\alpha)$ is a coefficient to be found by applying continuity conditions. Now differentiating (18) with respect to r and using (9), we get

$$G^+(r,\alpha)=\frac{1}{K\,J_1(Kb)}\left[-\dot{F}^+(b,\alpha)\,J_0(Kr)+\int_0^a \mathrm{d}r'\,r'\Big(f(r')-\mathrm{i}\alpha g(r')\Big)\,Q(r',r,\alpha)\right]. \tag{19}$$

The $G^+(r,\alpha)$ function is analytic in the upper half-plane. Taking into account that $K\,J_1(Kb)$ has zeros in this upper plane and taking into account the polar contributions coming from $\alpha=\alpha_m$, the following equation is obtained

$$\dot{F}^+(b,\alpha_m)=\frac{b}{2}J_0(j_m)\left(f_m-\mathrm{i}\alpha_m g_m\right) \tag{20}$$

with

$$\begin{aligned} f_m&=\tfrac{2}{b^2J_0^2(j_m)}\int_0^a \mathrm{d}r\,r\,f(r)J_0(j_m r/b),\\ g_m&=\tfrac{2}{b^2J_0^2(j_m)}\int_0^a \mathrm{d}r\,r\,g(r)J_0(j_m r/b), \end{aligned} \tag{21}$$

where j_m's are the roots of the following equation

$$J_1(j_m)=0,\quad m=0,1,2,\ldots \tag{22}$$

and

$$\begin{aligned} &\alpha_m=\sqrt{k^2-(j_m/b)^2},\quad \alpha_0=k,\\ &\mathrm{Im}(\alpha_m)\geq \mathrm{Im}(k). \end{aligned} \tag{23}$$

Note that when $m=0$, $J_0(j_0)=1$. By using (9) and taking into account (14)–(19), we obtain

$$\frac{\dot{F}^+(b,\alpha)}{K^2(\alpha)\,M(\alpha)}-\frac{b}{2}F^-(b,\alpha)=\frac{1}{2KJ_1(Kb)}\int_0^a \mathrm{d}r\,r\big(f(r)-\mathrm{i}\alpha g(r)\big)\,J_0(Kr), \tag{24}$$

where

$$M(\alpha)=\pi\,\mathrm{i}\,J_1(Kb)\;H_1^{(1)}(Kb). \tag{25}$$

Through (21), $f(r)$ and $g(r)$ can be expanded to the Dini series as given below

$$\begin{aligned} f(r)&=\sum_{m=0}^\infty f_m J_0(j_m r/b),\\ g(r)&=\sum_{m=0}^\infty g_m J_0(j_m r/b). \end{aligned} \tag{26}$$

By substituting (26) in (24) and computing the resulting integrals, the Wiener–Hopf equation is obtained as

$$\frac{\dot{F}^+(b,\alpha)}{K^2(\alpha)\,M(\alpha)}-\frac{b}{2}F^-(a,\alpha)=\frac{b}{2}\sum_{m=0}^\infty \frac{J_0(j_m)}{\alpha_m^2-\alpha^2}\Big(f_m-\mathrm{i}\alpha g_m\Big), \tag{27}$$

where $M(\alpha)$ can be written as [18]

$$\begin{aligned} M(\alpha)&=M_+(\alpha)\,M_-(\alpha),\\ M_-(\alpha)&=M_+(-\alpha). \end{aligned} \tag{28}$$

Here $M_+(\alpha)$ is analytic in the upper half-plane and $M_-(\alpha)$ is analytic in the lower half-plane. The explicit expression of $M_+(\alpha)$ is given in [18]. By multiplying (27) by $(k-\alpha)\,M_-(\alpha)$ and using the Wiener–Hopf method, the solution is easy to find [14], namely

$$\frac{\dot{F}^+(b,\alpha)}{(k+\alpha)\,M_+(\alpha)}=\frac{b}{2}\sum_{m=0}^\infty \frac{(k+\alpha_m)\,J_0(j_m)\,M_+(\alpha_m)\,(f_m+\mathrm{i}\alpha_m g_m)}{2\alpha_m(\alpha+\alpha_m)}. \tag{29}$$

4. Determination of the coefficients

The field in the region $\{r<a,\ -l<z<0\}$ can be written as follows [18]

$$\psi_3(r,z)=\sum_{n=1}^\infty A_n\left(\mathrm{e}^{-\mathrm{i}\tau_n z}+R_n\,\mathrm{e}^{\mathrm{i}\tau_n z}\right)J_0(\xi_n r/a), \tag{30}$$

where

$$\frac{\mathrm{i}ka}{Z_1}J_0(\xi_n)+\xi_n J_1(\xi_n)=0, \tag{31}$$

$$R_n=-\frac{1/Z_2-\tau_n/k}{1/Z_2+\tau_n/k}\,\mathrm{e}^{2\mathrm{i}\tau_n l} \tag{32}$$

and $\tau_n=\sqrt{k^2-(\xi_n/a)^2}$. Complex zeros of (31) can be found by different methods. The Newton method

is used in this study. The most important point in this method is the correct selection of the initial approach. Otherwise, some complex zeros may not be found and erroneous results may be obtained. The choice of the initial approach is made by utilizing the asymptotic behavior of ξ_n.

Consider now the continuity relation in (10), (11) using (17), (26) to obtain

$$\sum_{m=0}^{\infty} f_m J_0\left(j_m r/b\right) = \begin{cases} \mathrm{i}\sum\limits_{n=1}^{\infty} \tau_n A_n\left(R_n-1\right)\, J_0\left(\xi_n r/a\right) + \mathrm{i}k, & r<a, \\ 0, & a<r<b, \end{cases} \tag{33}$$

$$\sum_{m=0}^{\infty} g_m J_0\left(j_m r/b\right) = \sum_{n=1}^{\infty} A_n\left(R_n+1\right)\, J_0\left(\xi_n r/a\right) - 1, \quad r<a. \tag{34}$$

Multiplying both sides of (33) by $rJ_0\left(j_s r/b\right)$ and integrating from $r=0$ to $r=b$, we get

- for $n=0$

$$f_0 - \frac{2\mathrm{i}a^2}{b^2}\sum_{m=1}^{\infty}\frac{A_m\tau_m\left(R_m-1\right)J_1\left(\xi_m\right)}{\xi_m} = \frac{\mathrm{i}ka^2}{b^2}, \tag{35}$$

- for $n=1,2,\ldots$

$$f_n - \frac{2\mathrm{i}S_n}{b^2 J_0^2\left(j_n\right)}\sum_{m=1}^{\infty}\frac{A_m\tau_m\left(R_m-1\right)\xi_m J_1\left(\xi_m\right)}{\left(\xi_m/a\right)^2-\left(j_n/b\right)^2} = \frac{2\mathrm{i}kaJ_1\left(aj_n/b\right)}{bj_n J_0^2\left(j_n\right)}, \tag{36}$$

where

$$S_n = J_0\left(\frac{a}{b}j_n\right) + \frac{j_n Z_1}{\mathrm{i}kb}J_1\left(\frac{a}{b}j_n\right). \tag{37}$$

With a similar computation, i.e., multiplying (34) by $rJ_0\left(\xi_s r/a\right)$, the following equation is obtained

$$\sum_{m=0}^{\infty}\frac{g_m S_m}{\left(\xi_n/a\right)^2-\left(j_m/b\right)^2} - \frac{A_n\,\left(R_n+1\right)P_n}{\xi_n J_1\left(\xi_n\right)} = -\frac{a^2}{\xi_n^2}, \tag{38}$$

where

$$P_n = \frac{a^2}{2}\left[J_0^2\left(\xi_n\right)+J_1^2\left(\xi_n\right)\right]. \tag{39}$$

Finally, by substituting $\alpha=\alpha_1,\alpha_2,\alpha_3,\ldots$ in (29) and taking into account (20), one obtains

$$\frac{J_0\left(j_n\right)}{\left(k+\alpha_n\right)M_+\left(\alpha_n\right)}\left[f_n - \mathrm{i}\alpha_n g_n\right] = \sum_{m=0}^{\infty}\frac{\left(k+\alpha_m\right)J_0\left(j_m\right)M_+\left(\alpha_m\right)}{2\alpha_m\left(\alpha_n+\alpha_m\right)}\left[f_m+\mathrm{i}\alpha_m g_m\right], \tag{40}$$

for $n=1,2,\ldots$. The infinite series obtained in (35), (36), (38), and (40) are truncated to a certain number (N), allowing us to find the f_n, g_n, and A_n coefficients that are required for the diffracted field phenomenon.

5. Far field

By taking the inverse Fourier transform of $F\left(r,\alpha\right)$, we find the diffracted field in the region $r>b$ with the help of (14),

$$\psi_1\left(r,z\right) = -\frac{1}{2\pi}\int\limits_{\mathcal{L}}\mathrm{d}\alpha\,\frac{\dot{F}^+\left(b,\alpha\right)H_0^{(1)}\left(Kr\right)}{K\,H_1^{(1)}\left(Kb\right)}\,\mathrm{e}^{-\mathrm{i}\alpha z}, \tag{41}$$

where $\mathcal{L}$ is a straight line $\mathrm{Im}(-k)<\mathrm{Im}(\alpha)<\mathrm{Im}(k)$ parallel to the α-axis. Let us consider the asymptotic expansion of $H_0^{(1)}\left(Kr\right)$ as $kr\to\infty$, i.e.,

$$H_0^{(1)}\left(Kr\right) = \sqrt{\frac{2}{\pi Kr}}\,\mathrm{e}^{\mathrm{i}Kr-\mathrm{i}\pi/4} \tag{42}$$

with the substitutions given below as

$$r = R\sin(\theta), \quad z = R\cos(\theta). \tag{43}$$

The solution can be obtained using the saddle point formula

$$\psi_1\left(R,\theta\right) \sim D\left(\theta\right)\frac{\mathrm{e}^{\mathrm{i}kR}}{kR}, \tag{44}$$

where

$$D\left(\theta\right) = \frac{\mathrm{i}}{\pi\,\sin(\theta)}\,\frac{\dot{F}^+\left(b,-k\cos(\theta)\right)}{H_1^{(1)}\left(kb\sin(\theta)\right)}. \tag{45}$$

Here R and θ denote spherical coordinates.

6. Numerical results

To show the effects of parameters such as wall thickness and cavity depth on the diffraction field phenomenon, we present some computational results. The quantities ka, kb, and kl used in this paper are made dimensionless. Since the unit of the wave number k is 1/meter, the unit of the radius a, b and the length of the cavity is meter, then ka, kb, and kl are non-dimensional.

The expression given below is used to produce graphical plots for the diffracted field, i.e.,

$$\text{diffracted field} = 20\log\left|D\left(\theta\right)\right|. \tag{46}$$

The problem parameters are chosen from the studies of [17, 18, 24] that exist in the literature.

Figure 2 displays the variation of the diffracted field against the truncation number for different values of the observation angle. Since there is no contribution from some N values, $N=10$ is taken for the numerical computations.

Figures 3 and 4 show the variation of the amplitude of the diffracted field against the observation angle for different wall thickness values. As expected, the amplitude of the diffracted field

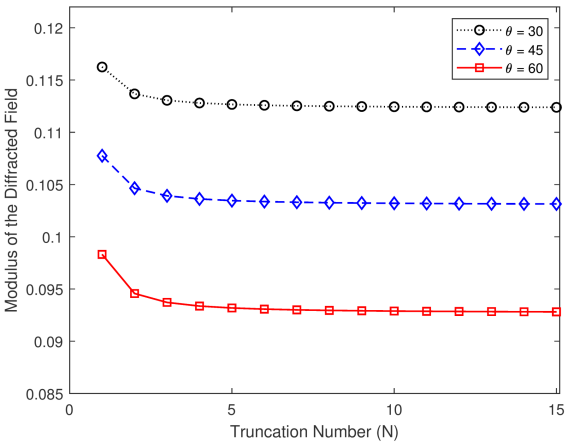

Fig. 2. Diffracted field against truncation number N for different values of the observation angle θ for $Z_1 = 1 + 1\mathrm{i}$, $Z_2 = 1 + 2\mathrm{i}$, $ka = 1$, $kb = 1.5$, $kl = 10$.

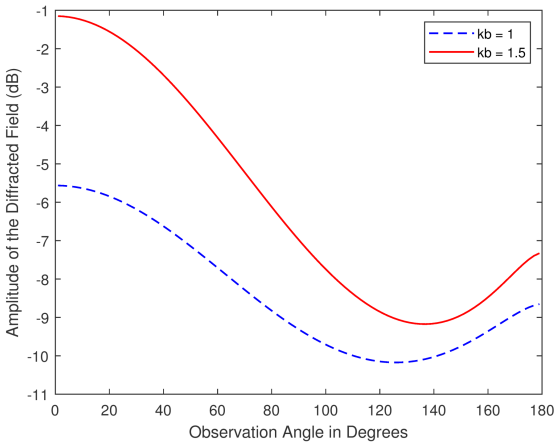

Fig. 3. Amplitude of the diffracted field for rigid cavity with different values of the wall thickness for $Z_1, Z_2 \to \infty$, $ka = 1$, $kl = 10$.

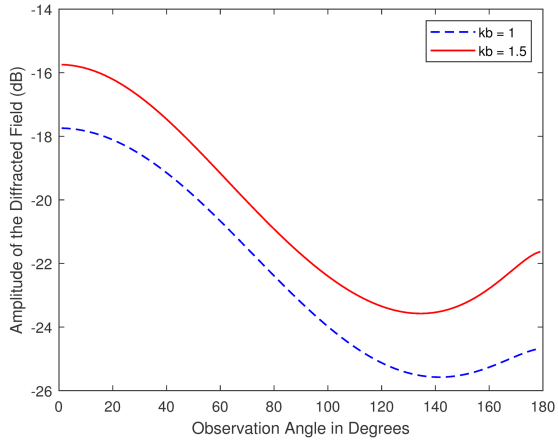

Fig. 4. Amplitude of the diffracted field for lined cavity with different values of the wall thickness for $Z_1 = 1 + 1\mathrm{i}$, $Z_2 = 1 + 2\mathrm{i}$, $ka = 1$, $kl = 10$.

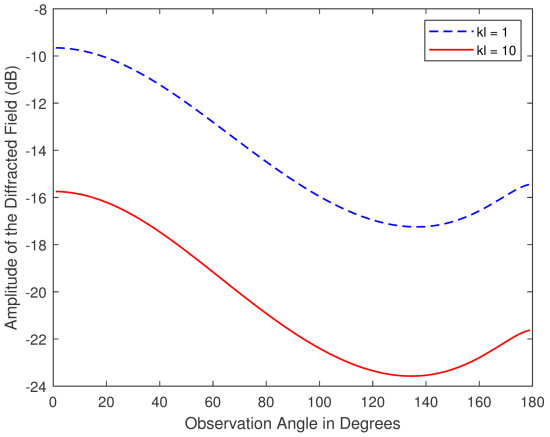

Fig. 5. Amplitude of the diffracted field for different values of the cavity depth for $Z_1 = 1 + 1\mathrm{i}$, $Z_2 = 1 + 2\mathrm{i}$, $ka = 1$, $kb = 1.5$.

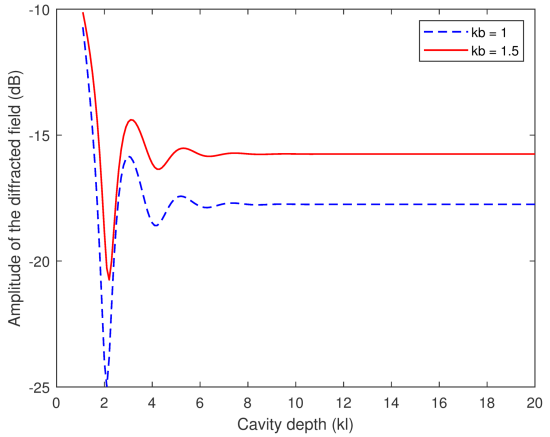

Fig. 6. Amplitude of the diffracted field against the cavity depth for $Z_1 = 1 + 1\mathrm{i}, Z_2 = 1 + 2\mathrm{i}$, $ka = 1$, $\theta = 2.2°$.

increases with increasing value of the wall thickness. These results clearly display the importance of the contribution of the wall thickness of the pipe to the diffraction phenomenon in realistic modeling. In Fig. 3, the walls of the cavity are taken as completely rigid. The amplitude of the diffracted field is shown for $Z_1, Z_2 \to \infty$. In Fig. 4, the different absorbing lining is considered, and $Z_1 = 1 + 1\mathrm{i}$, $Z_2 = 1 + 2\mathrm{i}$ are used.

Figure 5 displays the amplitude of the diffracted field variation against the observation angle for different values of the cavity depth. The amplitude of the diffracted field decreases with increasing values of kl. In Fig. 5, the parameters are taken as $ka = 1$, $kb = 1.5$, $Z_1 = 1 + 1\mathrm{i}$ and $Z_2 = 1 + 2\mathrm{i}$.

Figure 6 displays the effect of the cavity depth on the diffraction phenomenon for different values of the wall thickness. As in Figs. 3 and 4, the amplitude of the diffracted field increases as the wall thickness increases. It is also observed that the diffracted field obtained in Fig. 6 is almost constant (no resonance effect) for $kl > 6$.

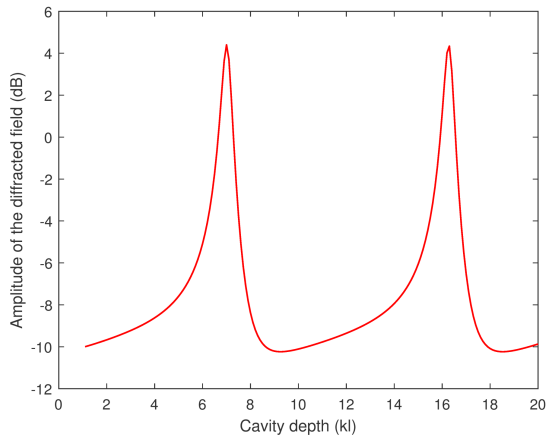

Fig. 7. Comparison of the cavity depth with the study of [18] for $Z_1^{-1} = Z_2^{-1} = 0.5\mathrm{i}$, $ka = kb = 1$, $\theta = 2.2°$.

The current problem was compared with a similar geometry (infinitely thin wall) [18] that exists in the literature. Figure 7 shows that the computational results obtained for close values of the parameters are consistent, which indicates the accuracy of the results obtained in this study. It can be seen that when the wall thickness goes to zero, the curve corresponding to $kb = ka$ gives the same result as the curve obtained in [18] (Fig. 7c).

7. Conclusions

The diffraction of sound waves from a cavity located in a semi-infinite pipe with a wall thickness is presented. It is assumed that the inner and base surfaces of the cavity are lined with an acoustically absorbent lining. The Wiener–Hopf technique is used to obtain the diffraction field. In this study, it is also assumed that the pipe wall is not infinitely thin, which makes the problem more realistic and complicated. The resulting complex expressions are meticulously examined, and the problem is solved analytically. The results obtained for some parameters of the problem are analyzed with graphs. It has also been observed that the effect of wall thickness on the diffraction phenomenon is remarkable.

References

[1] R.M. Munt, *J. Fluid Mech.* **83**, 609 (1977).

[2] G. Gabard, R.J. Astley, *J. Fluid Mech.* **549**, 315 (2006).

[3] S.W. Rienstra, *J. Eng. Math.* **59**, 451 (2007).

[4] A. Demir, S.W. Rienstra, in: *AIAA/CEAS Aeroacoustics Conf.*, Stockholm 2010, p. 3947.

[5] N. Peake, I.D. Abrahams, *Wave Motion* **92**, 102407 (2020).

[6] R. Sugimoto, P. Murray, R.J. Astley, in: *AIAA/CEAS Aeroacoustics Conf.*, Colorado Springs (CO) 2012 p. 2291.

[7] D.B. Kuryliak, Z.T. Nazarchuk, B.O. Trishchuk, *Prog. Electromagn. Res. B* **73**, 1 (2017).

[8] Hongli Ji, Xiaodong Wang, Jinhao Qiu, Li Cheng, Yipeng Wu, Chao Zhang, *J. Sound Vib.* **455**, 324 (2019).

[9] Jingwen Guo, Yi Fang, Ziyan Jiang, Xin Zhanga, *J. Acoust. Soc. Am.* **149**, 70 (2021).

[10] J. Jurkiewicz, A. Snakowska, D. Smolik, *Acta Phys. Pol. A* **119**, 1061 (2011).

[11] A. Snakowska, J. Jurkiewicz, L. Gorazd, *J. Sound Vib.* **396**, 325 (2017).

[12] A. Snakowska, J. Jurkiewicz, *J. Sound Vib.* **490**, 115722 (2021).

[13] H. Levine, J. Schwinger, *Phys. Rev.* **73**, 383 (1948).

[14] B. Noble, *Methods Based on the Wiener–Hopf Technique for the Solution of Partial Differential Equations*, Pergamon Press, 1958.

[15] Y. Ando, *Acta Acust. United Acust.* **22**, 219 (1969).

[16] A.D. Rawlins, *Proc. R. Soc. A: Math. Phys. Eng. Sci.* **361**, 65 (1978).

[17] A. Buyukaksoy, B. Polat, *J. Eng. Math.* **33**, 333 (1998).

[18] A. Demir, A. Buyukaksoy, B. Polat, *ZAMM* **82**, 619 (2002).

[19] B. Veitch, N. Peake, *J. Fluid Mech.* **613**, 275 (2008).

[20] B. Tiryakioglu, *Acta Acust United Acust.* **105**, 591 (2019).

[21] S. Shafique, M. Afzal, R. Nawaz, *Math. Mech. Solids* **25**, 1831 (2020).

[22] B. Tiryakioglu, A. Tiryakioglu, *IMA J. Appl. Math.* **86**, 828 (2021).

[23] B. Tiryakioglu, *J. Eng. Math.* **122**, 17 (2020).

[24] B. Tiryakioglu, *Int. J. Aeroacoustics* **19**, 38 (2020).